ISSN 1674-1056
http://cpb.iphy.ac.cn
http://iopscience.iop.org/cpb
中国物理 B
Chinese Physics
中国物理
Chinese Physics B

Propagation characteristics of parallel dark solitons in silicon-on-insulator waveguide

Zhen Liu(刘振), Weiguo Jia(贾维国), Yang Wang(汪洋), Hongyu Wang(王红玉), Neimule Men-Ke(门克内木乐), Jun-Ping Zhang(张俊萍)

Citation: Chin. Phys. B . 2020, 29(1): 014203 . **doi:** 10.1088/1674-1056/ab577d
Journal homepage: http://cpb.iphy.ac.cn; http://iopscience.iop.org/cpb

What follows is a list of articles you may be interested in

Unconventional phase transition of phase-change-memory materials for optical data storage

Nian-Ke Chen(陈念科), Xian-Bin Li(李贤斌)

Chin. Phys. B . 2019, 28(10): 104202 . **doi:** 10.1088/1674-1056/ab3cc3

Generation of breathing solitons in the propagation and interactions of Airy-Gaussian beams in a cubic-quintic nonlinear medium

Weijun Chen(陈卫军), Ying Ju(鞠莹), Chunyang Liu(刘春阳), Liankai Wang(王连锴), Keqing Lu(卢克清)

Chin. Phys. B . 2018, 27(11): 114216 . **doi:** 10.1088/1674-1056/27/11/114216

Three-dimensional modulations on the states of polarization of light fields

Peng Li(李鹏), Dongjing Wu(吴东京), Sheng Liu(刘圣), Yi Zhang(章毅), Xuyue Guo(郭旭岳), Shuxia Qi(齐淑霞), Yu Li(李渝), Jianlin Zhao(赵建林)

Chin. Phys. B . 2018, 27(11): 114201 . **doi:** 10.1088/1674-1056/27/11/114201

Enhancement and modulation of terahertz radiation by multi-color laser pulses

Min-Jie Pei(裴敏洁), Chen-Hui Lu(卢晨晖), Xian-Wei Wang(王宪位), Zhen-Rong Sun(孙真荣), Shi-An Zhang(张诗按)

Chin. Phys. B . 2018, 27(8): 084209 . **doi:** 10.1088/1674-1056/27/8/084209

Nonlinear effect of the structured light profilometry in the phase-shifting method and error correction

Zhang Wan-Zhen, Chen Zhe-Bo, Xia Bin-Feng, Lin Bin, Cao Xiang-Qun

Chin. Phys. B . 2014, 23(4): 044212 . **doi:** 10.1088/1674-1056/23/4/044212

Propagation characteristics of parallel dark solitons in silicon-on-insulator waveguide*

Zhen Liu(刘振), Weiguo Jia(贾维国)†, Yang Wang(汪洋), Hongyu Wang(王红玉), Neimule Men-Ke(门克内木乐), and Jun-Ping Zhang(张俊萍)

School of Physical Science and Technology, Inner Mongolia University, Hohhot 010021 *China*

(Received 16 August 2019; revised manuscript received 13 September 2019; accepted manuscript online 14 November 2019)

The propagation characteristic of two identical and parallel dark solitons in a silicon-on-insulator (SOI) waveguide is simulated numerically using the split-step Fourier method. The parallel dark solitons imposed by the initial chirp are investigated mainly by changing their power, their relative time delay. The simulation shows that the time delay deforms the parallel dark soliton pulse, forming a bright-like soliton in the transmission process and making the transmission quality down. By increasing the power of one dark soliton, the energy of the other dark soliton can be increased, and larger increase in a soliton's power leads to larger increase in the energy of the other. When the initial chirp is introduced into one of the dark solitons, higher energy consumption is observed. In particular, positive chirps resulting in pulse broadening width while negative chirps narrowing, with an obvious compression effect on the other dark soliton. Finally, large negative chirps are found to have a profound impact on parallel and nonparallel dark solitons.

Keywords: silicon-based optical waveguide, dark soliton, nonlinear effect, interaction

PACS: 42.65.Tg, 42.65.–k, 73.40.Qv, 42.25.Bs **DOI:** 10.1088/1674-1056/ab577d

1. Introduction

Silicon-on-insulator (SOI) waveguides are the main media used for silicon photonics research.[1] Because of the refractive index mismatch in the SOI waveguide core layer, light can be restricted to a small core layer, resulting in strong nonlinear optical effect, which enables us to realize a variety of optical functions in a very short length. It is expected that optical integrated chips will replace traditional chips and improve operational efficiency.[1–6] As integrated optical devices, SOI waveguides provide many advantages over traditional optical materials from production to applications. Firstly, the fabrication process of SOI devices is compatible with that of standard silicon complementary metal oxide semiconductors (CMOSs),[1,2] which has low costs and large scale. Secondly, SOI devices have a small size, small loss, good mode characteristics and polarisation, large transmission bandwidth, good thermal conductivity, and fast transmission speed.[6] Thirdly, they exhibit optical effects such as two-photon absorption, free-carrier absorption, and dispersion, which do not occur in traditional waveguides.[6,7] These advantages have led to recent advances in optical detectors[8] and photodiodes.[9] Design of ridge waveguides allows a quicker dissipation of free carriers, thus reducing their effect, and can combine metal p–i–n and waveguide structures, facilitating voltage loading.[10]

A dark soliton is a local pulse whose intensity decreases rapidly in the continuous wave background. Dark soliton pulses are stable and highly resistant to noise and losses in waveguides. Dark solitons have smaller amplitude attenuation rate, pulse width growth rate, and Gordon–Haus effect[11] than bright solitons,[12–16] and exhibit high code rate and good self-recovery. Therefore, they have attractive prospects in long-distance and large-capacity communication. Since 1987, dark soliton pulses have been transmitted successfully in optical fibres,[17] fibre lasers,[18,19] and quantum dot lasers.[20] Today, their transmission in SOI devices is actively studied. In this paper, two parallel dark solitons' transmission characteristics are simulated by MatLab. We study and illustrate the new pulse characteristics which are different from previous studies. The new pulse states of parallel dark solitons in SOI with different time delays, powers and chirps are investigated.

2. Theoretical model

The interaction characteristics of co-directional pulses transmitted in SOI devices can be expressed by the following nonlinear Schrödinger equations:[21–23]

$$\frac{\partial A_1}{\partial z}+\frac{\mathrm{i}}{2}\beta_2\frac{\partial^2 A_1}{\partial T^2}-\frac{1}{6}\beta_3\frac{\partial^3 A_1}{\partial T^3}=-\frac{1}{2}(\alpha_\mathrm{l}+\alpha_\mathrm{fc})A_1+\mathrm{i}k_0 n_\mathrm{fc}A_1 +\mathrm{i}\gamma\left(1+\frac{\mathrm{i}}{\omega_0}\frac{\partial}{\partial T}\right)\left(\frac{1+\rho}{2}|A_1|^2+\frac{2\rho}{3}|A_2|^2\right)A_1, \quad (1a)$$

$$\frac{\partial A_2}{\partial z}+\frac{\mathrm{i}}{2}\beta_2\frac{\partial^2 A_2}{\partial T^2}-\frac{1}{6}\beta_3\frac{\partial^3 A_2}{\partial T^3}=-\frac{1}{2}(\alpha_\mathrm{l}+\alpha_\mathrm{fc})A_2+\mathrm{i}k_0 n_\mathrm{fc}A_2 +\mathrm{i}\gamma\left(1+\frac{\mathrm{i}}{\omega_0}\frac{\partial}{\partial T}\right)\left(|A_2|^2+\frac{2}{3}\rho|A_1|^2\right)A_2, \quad (1b)$$

*Project supported by the National Natural Science Foundation of China (Grant No. 61741509).

†Corresponding author. E-mail: jwg1960@163.com

© 2020 Chinese Physical Society and IOP Publishing Ltd

where A_1 and A_2 are the slow-varying envelope amplitudes of the input waves in the same direction, z is the transmission distance, β_2 and β_3 are the dispersion coefficients of second and third orders, respectively, T is the time parameter under the reference frame of the group velocity, k_0 is the wave vector, α_l is the linear loss coefficient, with a numerical value of 0.2 dB/cm, α_{fc} is the free carrier loss coefficient, which can be obtained from the formula $\alpha_{fc} = \sigma N_C$, and $\sigma \approx 1.45 \times 10^{-21}$ m^2 is the free carrier absorption coefficient. Here n_{fc} is the change in refractive index caused by a free carrier, which can be obtained from the formula $n_{fc} = 2k_c N_C$, and $k_c = 1.35 \times 10^{-27}$ m is the wavenumber of the free carrier; γ is the nonlinear coefficient obtained from the formula $\gamma = n_2 k_0 / A_{eff} + i\beta_{TPA}/A_{eff}$, and $n_2 \approx 6 \times 10^{-18}$ m^2/W is the Kerr coefficient. Finally, N_C is the average free carrier concentration generated by two-photon absorption. The average free carrier concentration evolution is described by the following equation:[24]

$$\frac{dN_C(z,T)}{dT} = \frac{\beta_{TPA}}{2h\nu_0 A_{eff}^2} |A(z,T)|^4 - \frac{N_C(z,T)}{\tau_{eff}}, \quad (2)$$

where h is the Planck constant, ν_0 is the photon frequency, β_{TPA} is the two-photon absorption coefficient, A_{eff} is the effective module area, $A(zT)$ is the total field distribution, and τ_{eff} is the free carrier lifetime. The nonlinear effects in a waveguide are mainly the Kerr effect and two-photon absorption. Because the pulse width is larger than 100 fs, dispersions above the third order and the self-steepening effect of the Raman sum are not discussed. The parameter ρ is the silicon material property parameter, and its numerical value is 1.27.

3. Numerical simulation and analysis

The numerical simulation of a ridge SOI was carried out based on the waveguide structure shown in Fig. 1. The incident light propagates along the z-axis of the waveguide with polarization along the x-axis, satisfying the condition of normal dispersion. We selected waveguide length $L = 5$ mm, width $W = 1$ μm, height $H = 0.6$ μm, and etching depth $h = 0.3$ μm to ensure the accuracy of simulation. The initial input pulse is produced by two-dark solitons of the same frequency; the pulse wavelength is $\lambda = 1550$ nm and the pulse width is 250 fs.

The two-pulse envelope waveforms can be expressed as follows:

$$A_1 = \sqrt{P_1}\tanh((T - \tau/2)/T_0),$$
$$A_2 = \sqrt{P_2}\tanh((T + \tau/2)/T_0),$$

where P_1 and P_2 are the input powers of the two input pulses, τ is the time delay between the two input pulses, and T_0 is the pulse width. The set parameters are as follows: $\beta_2 = 30$ ps^2/m, $\beta_3 = 0.6$ ps^3/m, $\tau_{eff} = 1$ ns, and $\beta_{TPA} = 5 \times 10^{12}$ m/W. The group refractive index in the x direction is $n = 3.26$ and the initial power is 20 W.

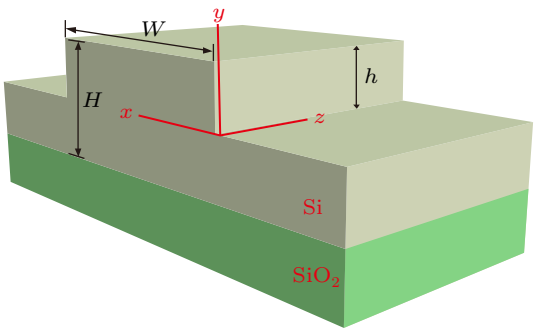


Fig. 1. Schematic of the silicon-based optical waveguide structure.

3.1. Effect of the time delay

The two dark soliton pulse width and input power are kept to be unchanged. Only the input time delay was changed and was selected as 0 ps, 0.3 ps, and 3 ps for the coaxial condition, small time delay, and large time delay, respectively. The time-domain transmission waveform obtained from the numerical simulation is shown in Fig. 2.

From Figs. 2(a) and 3(a), it can be seen that when the two solitons are coaxial, the background power of the coupled pulse increases to 40 W and then decreases rapidly due to the influence of two-photon and free-carrier absorptions. As the transmission distance increases, grey-like solitons appear on both sides, accompanied by front and rear edge oscillations. Dark solitons A_1 and A_2 also produce gray-like solitons, and A_2 has a narrower pulse and smaller oscillation than A_1. When the time delay is 0.3 ps, the initial background power of the coupled pulse is 40 W, but the initial blackness value of the coupled pulse is insufficient due to the time delay, the soliton becomes a grey one, and the pulse width is increased significantly. The hump at the trailing edge has a significant peak increase after transmitting a distance. During its transmission, the position of dark soliton A_1 is offset on both sides relative to that of the grey soliton. The peak value of the front hump is always higher than that of the back one, and bright solitons tend to be formed. The main pulse of A_2 is compressed and induced to move backward because the peak value of the back-edge hump increases in the first 2 mm. Consequently, the main pulse broadens and the energy concentrates at the back-edge hump. Between 2 mm and 5 mm, the main pulse and the rising back-edge hump are gradually affected by dispersion, the grey level and peak value are lost, and the total energy of the dark soliton A_2 is focused along the grey soliton and continues to be transmitted. As shown in Figs. 2(c2) and 2(c3), when $\tau = 3$ ps, A_1 and A_2 are transformed into light-dark solitons with a time delay, and the light-dark solitons have the same pulse width. From Figs. 3(c2) and 3(c3), it can be seen that the parallel pulses are bright-like solitons formed by the

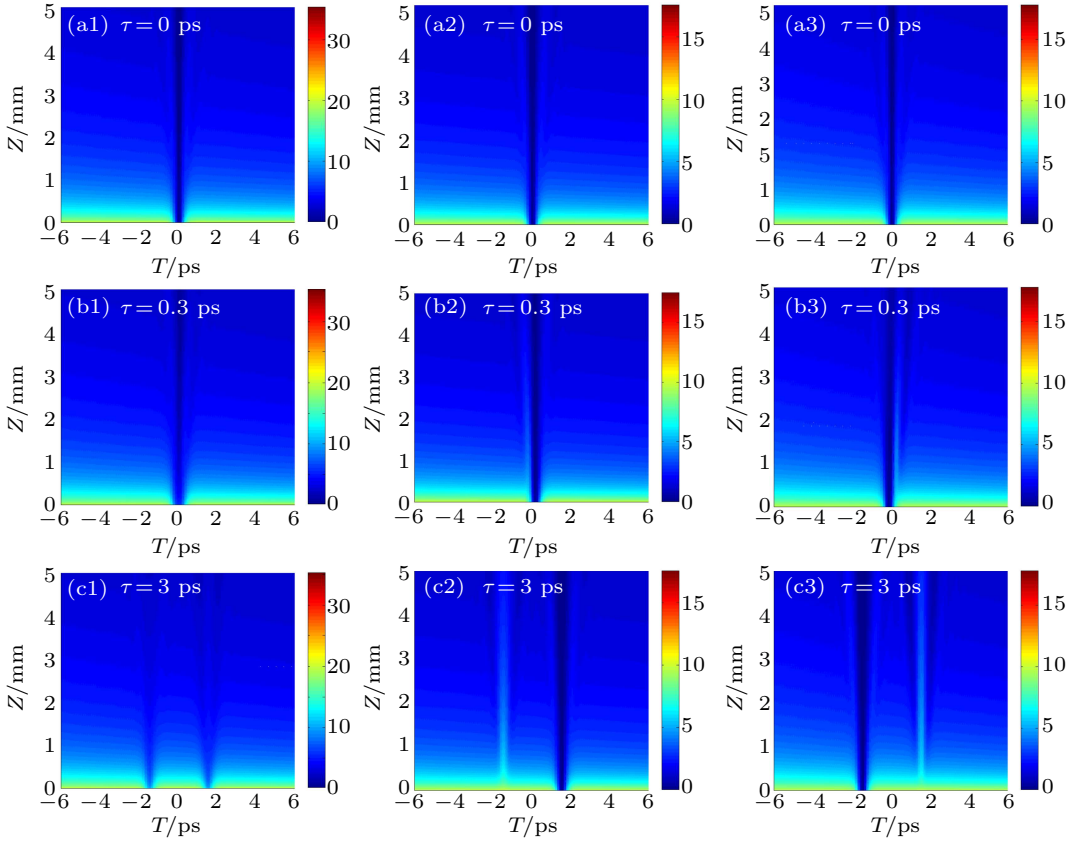


Fig. 2. The time-domain transmission of dark solitons with different time delays: (a) $\tau = 0$ ps, (b) $\tau = 0.3$ ps, (c) $\tau = 3$ ps, for (1) the two-pulse coupling waveforms, (2) the transmission waveform of dark solitons A_1 in the parallel transmission process, and (3) the transmission waveform of dark solitons A_2 in the parallel transmission process.

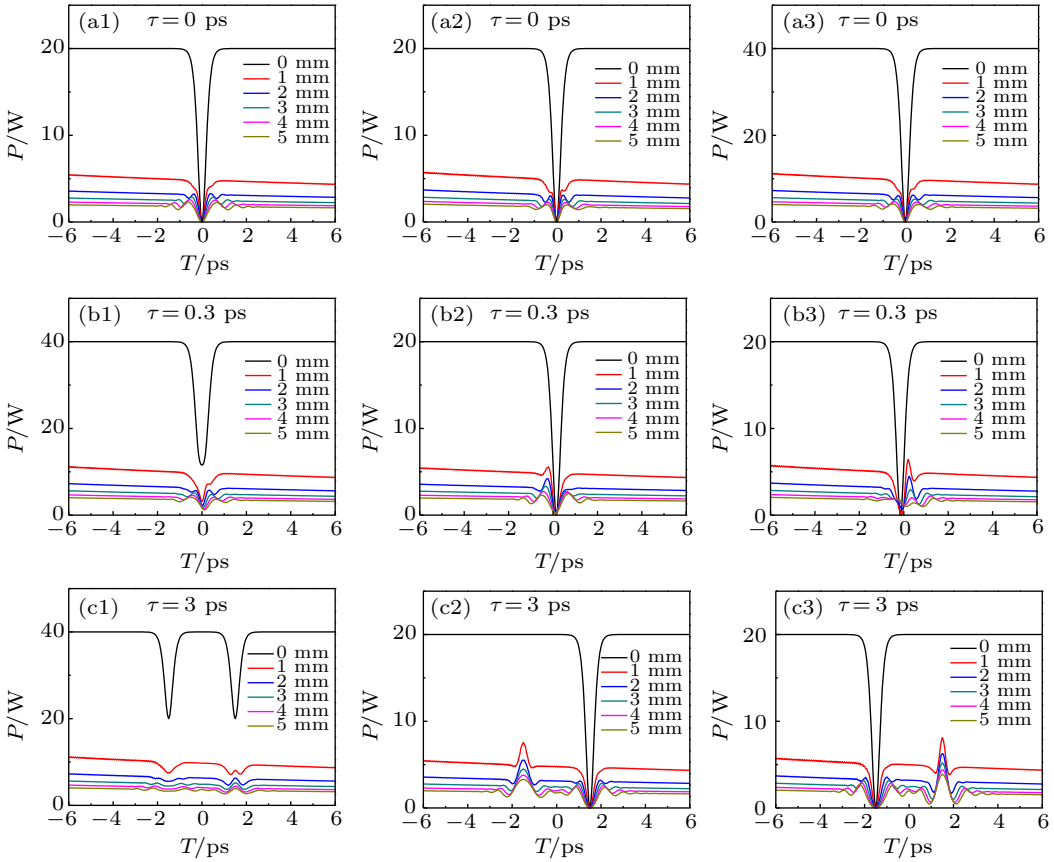


Fig. 3. The specific waveforms of the dark solitons at different distances with time delays (a) $\tau = 0$ ps, (b) $\tau = 0.3$ ps, (c) $\tau = 3$ ps for (1) a two-pulse coupled waveform, (2) the waveform of dark soliton A_1 in parallel transmission, (3) the waveform of dark soliton A_2 in parallel transmission.

coupling of dark solitons with the time parameter of the other dark soliton, similar to the rise of dark solitons along the hump under the condition of small time delay. Owing to dispersion, the bright and dark solitons broaden, and the trailing edge oscillation generated by the leading A_2 shifts to the trailing edge of the generated bright solitons. From Figs. 2(c1) and 3(c1), it can be seen that the coupled pulse changes into a parallel dark soliton with time delay under conditions. Owing to losses and nonlinear effects, the energy gradually loses and the grayscale decreases. By comparing Figs. 3(c2) and 3(c3), it can be observed that the peak value of the bright-like soliton produced by A_2 is significantly higher than that of A_1, so the coupling pulse eventually behaves as a bright soliton with greater time delay.

3.2. Influence of solitons power

In the simulation, we set the two dark solitons such that the zero-time-delay condition is maintained, kept the power of the dark soliton A_1 unchanged at 20 W, set the power of the dark soliton A_2 to 20 W, 40 W, and 60 W, and simulated the transmission waveform of dark soliton A_1. Then, we changed the power of dark soliton A_1 to 40 W and 60 W and simulated the transmission waveform of the dark soliton A_1 with the nine power combinations.

From Figs. 4(a1), 4(b1), and 4(c1), it can be seen that with increasing P_1, the background of dark soliton A_1 darkens and its energy decreases, which indicates that the two-photon absorption is affected by the power and has a significant influence on the energy of dark solitons. Figure 4 shows a comparison of the energy of dark soliton A_1 with different P_2 values and constant P_1 value. The figure shows that, as the power of dark soliton A_2 increases, the bright background area of dark soliton A_1 at different powers expands, which corresponds to an increase in its energy. As shown in Fig. 5, the waveform at 5 mm indicates that the overall energy of dark soliton A_1 is higher when the power of dark soliton A_2 is higher. The energy of A_1 is increased when P_2 increases from 20 W to 40 W; the change in P_2 has little effect on the waveform of A_1. Under different P_2 values, the peak value of the left and right humps of A_1 increase, the pulse width remains almost unchanged, and the back-edge oscillation waveform generated by third-order dispersion is almost identical. As shown in Fig. 6, the change in P_2 affects the decay trend in the A_1 energy significantly. When the P_2 value is relatively high, the average energy of A_1 at each distance is also high. The higher the P_2 value is, the greater the energy increase of A_1 is. The increase in P_2 from 20 W to 40 W for P_1 is significantly greater than that in P_2 from 40 W to 60 W.

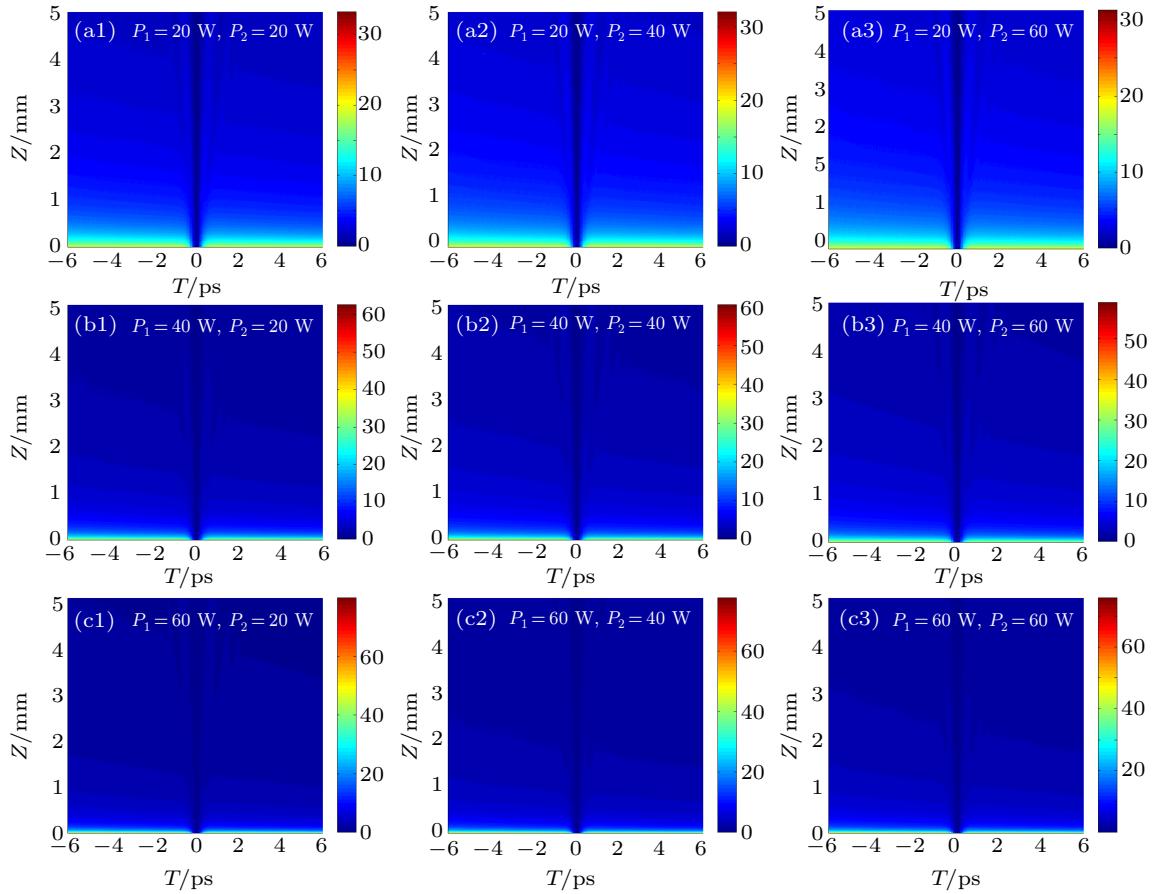


Fig. 4. Waveform of dark soliton A_1 with different values of P_2 for (a) $P_1 = 20$ W, (b) $P_1 = 40$ W, and (c) $P_1 = 60$ W.

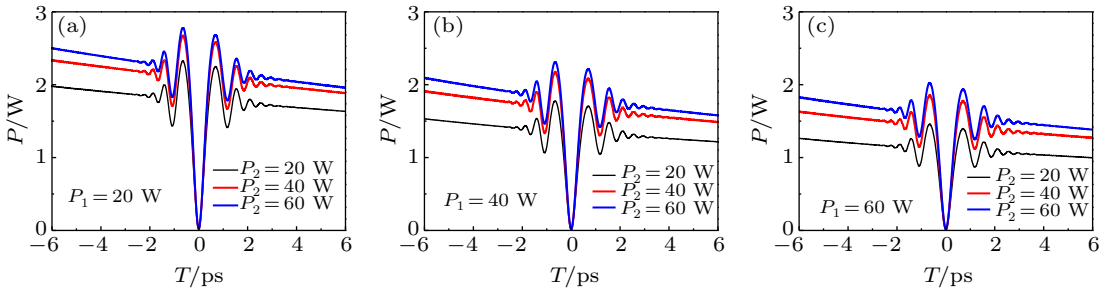


Fig. 5. Pulse waveform diagram of A_1 dark soliton at 5 mm for different P_1 and P_2.

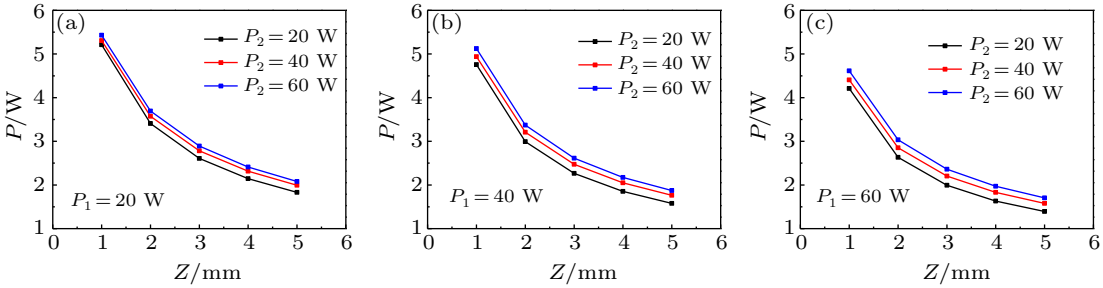


Fig. 6. Average energy variation of dark soliton A_1 at different distances for different P_1 and P_2.

3.3. The effect of chirp

To investigate its effects on the interaction between dark solitons, an initial chirp is introduced into the A_1 pulse. The waveform of dark soliton A_1 when the chirp is introduced can be expressed as

$$A_1 = \sqrt{P_1}\tanh(T/T_0)\exp\left(-\frac{\mathrm{i}CT^2}{2T_0^2}\right),$$

where C is the chirp parameter. The dark solitons are set to maintain the zero-time-delay condition, the initial power is set to $P_1 = P_2 = 20$ W, and different C values are taken to simulate the transmission waveform of A_1.

From Fig. 7(a), it can be seen that during the change in the C value from -0.2 to 0.2, the overall background of the dark soliton presents a dark-light-dark change trend, i.e., a low-high-low change in the transmitted pulse energy. From the comparison of the average energy at each transmission distance shown in Fig. 9(a) and the change in the A_1 energy at 5 mm shown in Fig. 9(c), it can be seen that chirp can cause the pulse to lose energy and that smaller absolute values of the chirp parameter cause smaller energy losses. We can compare the energy changes of dark soliton A_2 affected by different chirp parameters A_1 in Figs. 9(b) and 9(c). When A_1 is chirped, the energy of dark soliton A_2 changes much less than that of A_1. The energy at different transmission distances is almost constant, and the energy changes at 5 mm fluctuate slightly.

From Figs. 7 and 8, it can be seen that the dark soliton compresses first and then widens during transmission. Because the previous two-photon absorption is too intense, the energy consumption is too large for pulse width broadening, i.e., pulse compression. Because the two-photon absorption in the early stage is too intense and the energy consumption is too large for pulse width broadening, i.e., pulse compression, after the transmission exceeds 1 mm, the two-photon

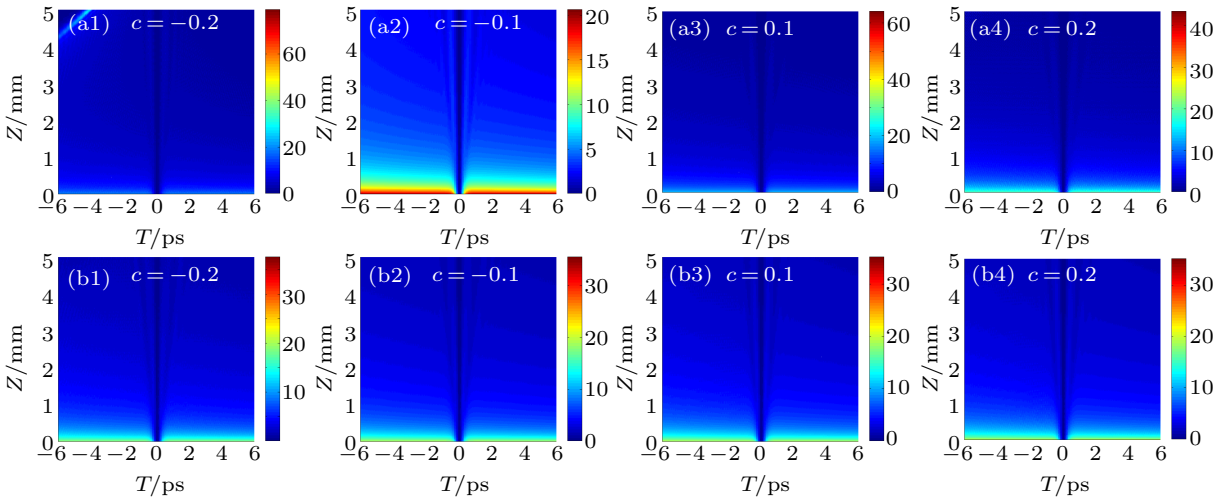


Fig. 7. (a) Transmission waveforms of dark soliton A_1 with different chirp parameters C and (b) parallel transmission waveforms of dark soliton A_2 with different C values of dark soliton A_1.

absorption decreases due to the energy reduction, and the dark soliton begins to broaden due to nonlinear effects. From Fig. 8(a), it can be seen that the pulse width of dark soliton A_1 with a chirp is larger than 250 fs after a 5-mm transmission. For the pulse width curve of dark soliton A_1, the positive chirp curve is above the zero-chirp curve and the negative chirp curve is below the zero-chirp curve. The distance between the negative chirp curve and the zero-chirp curve is determined by the absolute value of the chirp parameter. The larger the absolute value is, the closer the chirp curves are. This indicates that positive chirps promote pulse broadening, negative chirps inhibit pulse broadening, and larger absolute values of the chirp parameter cause stronger effects on dark solitons. As shown in Figs. 7(b) and 8(b), the amount of compression of dark soliton A_2 under the influence of different chirped dark solitons is larger than that of A_1. The compression distance of the A_2 pulse is longer than that of the A_1 pulse. Although the A_2 pulse broadens in the subsequent transmission process, its width is less than 250 fs at 5 mm. Furthermore, larger chirp parameter values lead to larger overall pulse widths. This indicates that, within 5 mm, when one of the two dark solitons in parallel transmission has a chirp, the other dark solitons are affected by the compression, and the smaller chirp parameters cause larger compressions.

From Fig. 7(a1), it can be seen that when the absolute value of the negative enthalpy parameter reaches a certain value, an interference wave similar to rogue solitons is generated. Rogue solitons have attracted extensive attention in optics[25–27] and fluid mechanics[28,29] in recent years. As shown in Fig. 10(c), the generated interference wave is a high-pulse single pulse, and the energy of the pulse front becomes 0. When the absolute value of the negative enthalpy parameter increases, the position of the interference wave moves towards that of the main dark soliton pulse. As shown in Fig. 10(a), when $C = -0.5$, A_1 intersects the interference wave at more than 3 mm, it is arc-shaped, and is transmitted over the dark soliton main pulse to the trailing edge. From Figs. 10(b) and 10(c), it can be seen that dark soliton A_2 is greatly affected by the strange wave at depths of more than 3 mm, and the effective transmission distance reduces and gradually becomes a small oscillation of the background energy.

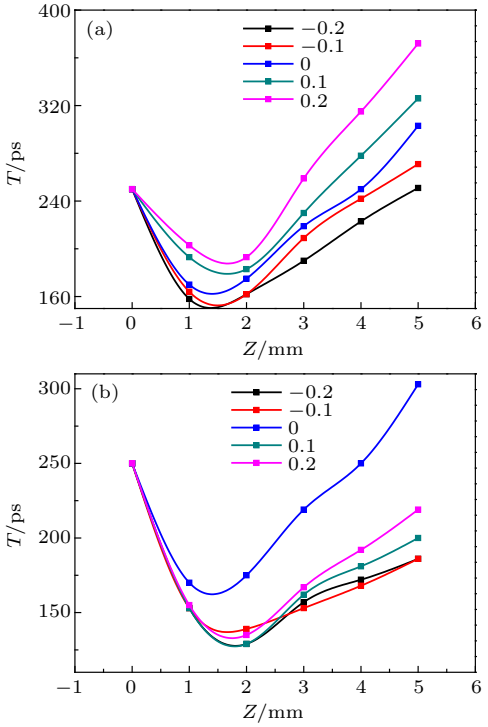


Fig. 8. Pulse width variation trend of dark soliton A_1 (a) and A_2 (b) transmitted to different distances with different C values.

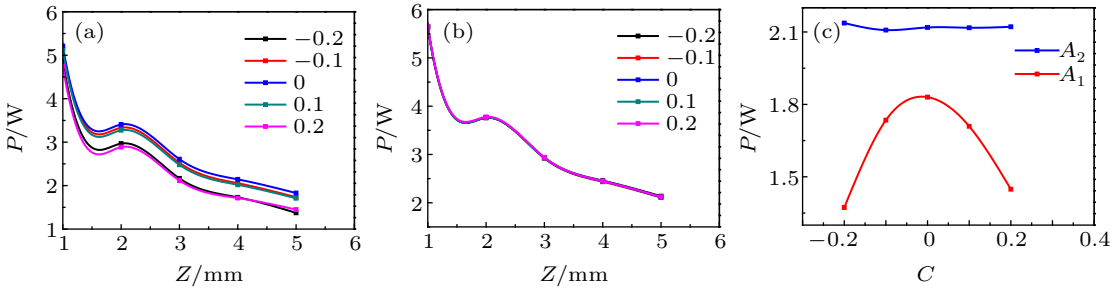


Fig. 9. Average energy change of dark solitons A_1 (a) and A_2 (b) with different C values. (c) Relationship between the average energy of dark solitons A_1 and A_2 at 5 mm as a function of the C values.

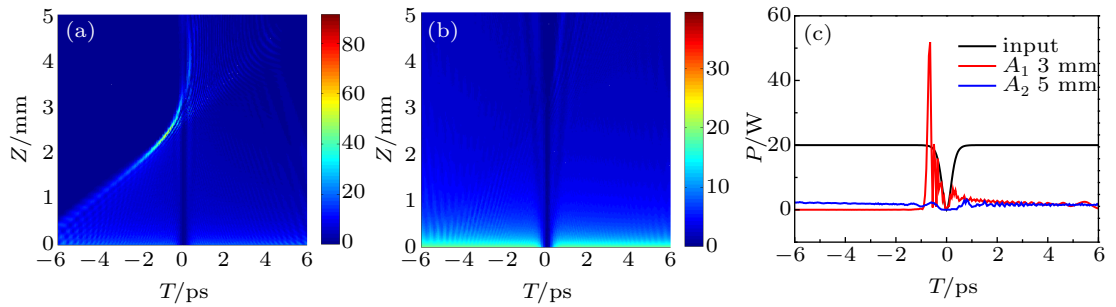


Fig. 10. Transmission waveform of dark solitons A_1 (a) and A_2 (b) generating interfering waves with $C = -0.5$. (c) Specific waveform comparison of input pulse with A_1 at 3 mm and A_2 at 5 mm.

4. Conclusion

Two parallel dark soliton pairs propagate differently in a silicon-based optical waveguide, with one dark soliton having a narrow pulse width and a small oscillation. By introducing a time delay, the original pulse shape of the input dark soliton disappears and a bright soliton-like pulse is generated, which will shorten the effective transmission distance of the dark soliton. The input power of one of the dark solitons affects the average energy of the other, with larger powers leading to higher energies of the other dark soliton and stronger lifting effects. If the value of chirp parameters increases, it will lead to larger broadenings and cause higher energy consumption. However, the energy of the parallel dark solitons has a slight impact, and the parallel dark soliton is compressed. Smaller chirp parameters lead to larger compressions. When a negative chirp is too large, a special interference wave will be generated in the dark soliton background, which will have destructive effects on the parallel dark solitons.

References

[1] Jalali B, Claps R, Dimitropoulos D and Raghunathan V 2004 *Topics in Applied Physics: Silicon Photonics* **94** 199

[2] Espinola R L, Dadap J I, Osgood R, Mcnab S J and Vlasov Y A 2004 *Opt. Express* **12** 3713

[3] Sih V, Xu S, Kuo Y H, Rong H, Paniccia M, Cohen O and Raday O 2007 *Opt. Express* **15** 357

[4] Först M, Niehusmann J, Plötzing T, Kurz H and Moormann C 2007 *Integr. Photon. Nanophoton.* 8–11 July 2007, Salt Lake City Utah United States) p IWD2

[5] Lu J Q, Jia W G and Chen R 2018 *J. Mod. Opt.* **65** 1793

[6] Jin W 2015 *Nonlinear Optical Effect and Application Based on SOI Waveguides* (Beijing: Publishing National Defense Industry) Vol. 1 pp. 12–23

[7] Liang T K, Tsang H K, Day I E, Drake J, Knights A P and Asghari M 2002 *Appl. Phys. Lett.* **81** 1323

[8] Han Z T, Chu J K, Men F T and Jin R C 2009 *J. Semiconduct.* **30** 104008

[9] Chu J, Han Z, Meng F and Wang Z 2011 *Solid-State Electron.* **55** 54

[10] Yin L H 2009 *PhD Dissertation* (New York: University of Rochester)

[11] Yao X L 2016 *Inner Mongolia Sci. Technol. & Economy* **15** 105 (in Chinese)

[12] Chen S S, Tian B, Liu L, Yuan Y Q and Zhang C R 2019 *Chaos Soliton. Fract* **118** 337

[13] Yu Y, Jia W G, Yan Q, Neimule M and Zhang J P 2015 *Acta Phys. Sin.* **64** 054207 (in Chinese)

[14] Yuan Y Q, Tian B, Liu L, Wu X Y and Sun Y 2018 *J. Math. Anal. Appl.* **460** 476

[15] Zhao X X, Tian B, Xie X Y, Wu X Y, Sun Y and Guo Y J 2018 *Wave. Random Complex* **28** 356

[16] Tiu Z C, Zarei A, Ahmad H and Harun S W 2016 *Chin. Phys. Lett.* **33** 034201

[17] Emplit P, Hamaide J P, Reynaud F, Froehly C and Barthelemy A 1987 *Opt. Commun.* **62** 374

[18] Tiu Z C, Zarei A, Tan S J, Ahmad H and Harun S W 2015 *Chin. Phys. Lett.* **32** 034203

[19] Zhang H, Tang D Y, Zhao L M and Wu X 2010 *Phys. Rev. A* **80** 045803

[20] Feng M, Silverman K L, Mirin R P and Cundiff S T 2010 *Opt. Express* **18** 13385

[21] Yin L H, Zhang J D, Fauchet P M and Agrawal G P 2009 *Opt. Lett.* **34** 476

[22] Chen R, Jia W G, Wang X Y, Zhang J P and Neimule M 2017 *J. Mod. Opt.* **64** 1809

[23] Chen R, Jia W G, Wang X Y and Lu J Q 2017 *J. Opt. Soc. Am. B* **34** 2295

[24] Wen J, Ma C J, Fan W and Fu H W 2015 *Opt. Laser Technol.* **71** 50

[25] Du Z, Tian B, Chai H P, Sun Y and Zhang X H 2018 *Chaos Soliton. Fract.* **109** 90

[26] Zhang C R, Tian B, Wu X Y, Yuan Y Q and Du X X 2018 *Phys. Scr.* **93** 095202

[27] Li Z D, Wang Y Y and He P B 2019 *Chin. Phys. B* **28** 010504

[28] Wang M, Tian B, Sun Y, Yin H M and Zhang Z 2019 *Chin. J. Phys.* **60** 440

[29] Hu C C, Tian B, Wu X Y, Yuan Y Q and Du Z 2018 *Eur. Phys. J. Plus* **133** 40